INSTITUTE OF PHYSICS PUBLISHING PHYSICS IN MEDICINE AND BIOLOGY

Phys. Med. Biol. **47** (2002) 3679–3689 PII: S0031-9155(02)52384-8

The development of terahertz sources and their applications

A G Davies, E H Linfield and M B Johnston

Cavendish Laboratory, University of Cambridge, Madingley Road, Cambridge CB3 0HE, UK

E-mail: agd11@cam.ac.uk (A G Davies)

Received 25 March 2002
Published 17 October 2002
Online at stacks.iop.org/PMB/47/3679

Abstract

The terahertz region of the electromagnetic spectrum spans the frequency range between the mid-infrared and the millimetre/microwave. This region has not been exploited fully to date owing to the limited number of suitable (in particular, coherent) radiation sources and detectors. Recent demonstrations, using pulsed near-infrared femtosecond laser systems, of the viability of THz medical imaging and spectroscopy have sparked international interest; yet much research still needs to be undertaken to optimize both the power and bandwidth in such THz systems. In this paper, we review how femtosecond near-infrared laser pulses can be converted into broad band THz radiation using semiconductor crystals, and discuss in depth the optimization of one specific generation mechanism based on ultra-fast transport of electrons and holes at a semiconductor surface. We also outline a few of the opportunities for a technology that can address a diverse range of challenges spanning the physical and biological sciences, and note the continuing need for the development of solid state, continuous wave, THz sources which operate at room temperature.

(Some figures in this article are in colour only in the electronic version)

1. Introduction

The terahertz (THz) frequency range, usually defined as 100 GHz–10 THz, represents a significant portion of the electromagnetic spectrum (figure 1), for which compact, solid-state sources that operate at room temperature are still not available.

On the microwave side of the spectrum, it is difficult to fabricate electronic devices that operate at frequencies substantially above a few hundred GHz [1] (although the output of such sources can be harmonically multiplied to the THz range [2]). This is partially a result of the inherent need for very short carrier transit times in the active regions and is also a consequence of only low powers being delivered by devices which must have small device areas to minimize the device capacitance.

 © 2002 IOP Publishing Ltd Printed in the UK

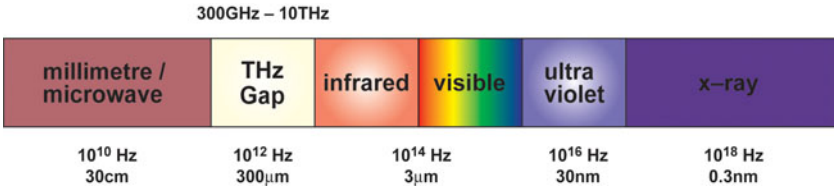

Figure 1. A schematic representation of the electromagnetic spectrum showing the THz region.

On the optical side of the spectrum, interband diode lasers have long been designed for operation at visible and near-infrared frequencies. However, this concept, where light is generated by the radiative recombination of conduction band electrons with valence band holes across the bandgap of the active material, cannot be simply extended into the mid-infrared since suitable semiconductors are not available. Instead, recent research has made extensive use of the quantum cascade (QC) concept in which inter-subband or inter-miniband transitions in layered semiconductor heterostructures are used to generate light in the mid-infrared region of the spectrum [3]. By appropriately engineering the thickness of the different semiconductor layers, the electron motion is confined along the growth direction, thereby splitting the conduction band into a number of discrete states. The corresponding electron transition energies can, in principle, be tailored to cover a wide range of wavelengths, from the far- to the mid-infrared, using InP- or GaAs-based III–V compounds.

These unipolar injection lasers, named 'quantum cascade' from the possibility of stacking together successive active regions to generate a multiplicity of photons for each injected electron, have been demonstrated at room temperature in the mid-infrared up to the longest wavelength of 24 μm (12.5 THz) [4]. However, extending this concept to frequencies below 10 THz is a considerable challenge: for example, free carrier absorption in semiconductors scales approximately as the wavelength squared requiring a large-gain active region, and the small energy (10–20 meV) of the optical transition necessitates very selective injection. Furthermore, there are difficulties in waveguiding THz radiation in an active material that is just a few microns thick, since a conventional dielectric waveguide using semiconductor cladding layers of smaller refractive index would not only require prohibitive thicknesses for molecular beam epitaxy (MBE) growth but would also result in small confinement factors. Despite these issues, THz QC lasers operating at 4.4 THz have recently been demonstrated [5, 6], but at present operation is confined to cryogenic temperatures.

Owing to the difficulties in fabricating solid-state THz sources, researchers have focused attention on all-optical techniques of producing THz radiation employing visible/near-infrared, femtosecond pulsed lasers. It is with these *coherent* THz systems that many of the exciting prototype experiments have been undertaken which have demonstrated the potential of THz radiation for imaging and spectroscopy in the biomedical sciences. In this paper, we will focus on such systems. We will review how semiconductor structures can be used to convert ultra-short ($\sim$100 fs) near-infrared pulses into THz pulses, and then concentrate our discussion on one THz generation mechanism based on the ultra-fast transport of electrons and holes at semiconductor surfaces. Although these broadband coherent THz systems have a wide range of potential applications, there remains a critical need for the development of solid-state sources and these must remain a focus for future research.

2. Coherent THz imaging and spectroscopy systems

A schematic representation of a THz time-domain spectroscopy system is shown in figure 2 [7] (for a detailed discussion, see [8]).

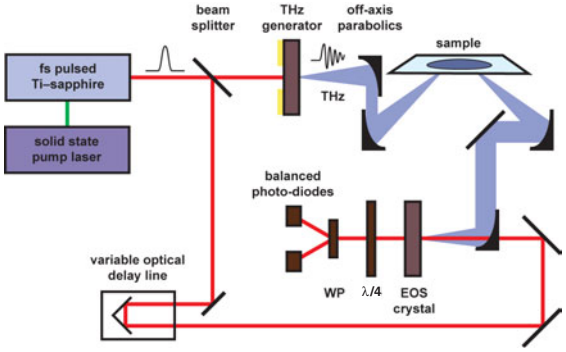

Figure 2. Schematic diagram of a THz time-domain spectroscopy system.

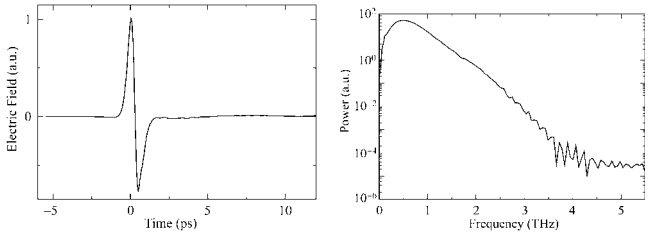

Figure 3. Example of a typical THz pulse in the time domain (left) and, after Fourier transformation, in the frequency domain (right).

Ultra-short (∼10–200 fs) visible/near-infrared pulses (typically centred at 780 nm) are directed onto a semiconductor THz generator which converts the incident pulses into THz pulses. The THz pulses are either emitted colinearly with the reflected incident pulses, or propagate through the semiconductor generator and emerge from the far side. The emitted THz radiation is collected and collimated by an off-axis parabolic mirror, and then focused by a second off-axis parabolic mirror onto the sample, which can be stepped across the beam to build up a two-dimensional image.

Coherent detection of the transmitted or reflected THz radiation can be achieved in a number of ways [8]. Figure 2 shows a technique based on the ultrafast Pockels effect [9] in which the THz beam is collected and focused onto an electro-optical sampling (EOS) detection crystal (for example, {110} ZnTe). The THz field induces an instantaneous birefringence in the electro-optic medium, which is readily probed with a second visible/near-infrared beam, initially split from the pump beam. The birefringence modulates the ellipticity of the probe beam, which is measured using a quarter waveplate ($\lambda/4$), a Wollaston polarization (WP) splitting prism, and two balanced photodiodes. By placing an acousto-optic modulator in the pump beam (not shown), lock-in techniques can be used to measure the photodiode signal. Furthermore, by measuring this signal as a function of the time-delay between the arrival of the THz and probe pulses at the EOS crystal, the electric field of the THz pulse in the time domain can be obtained (figure 3, left), and the Fourier transform gives the frequency spectrum of the THz radiation (figure 3, right).

3. THz semiconductor sources

Semiconductor surfaces have been widely used in conjunction with femtosecond visible/near-infrared lasers as THz emitters, exploiting bulk electro-optic rectification (difference-frequency mixing) and ultrafast charge transport techniques.

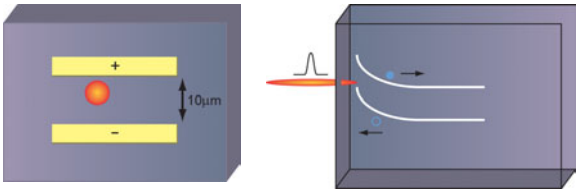

(a) (b)

Figure 4. Schematic diagrams showing two THz emitters in which photoexcited carriers generated by a focused visible/near-infrared laser pulse are accelerated and radiate in an electric field. In (a) the field is provided by a lateral antenna structure, in (b) the intrinsic semiconductor surface depletion/accumulation field is exploited.

3.1. Bulk electro-optic rectification

The large peak electric field of the visible/near-infrared pulse allows the second order nonlinear susceptibility ($\chi^{(2)}$) of a semiconductor crystal to be exploited for the generation of THz radiation. A time-dependent polarization is induced in the THz frequency range which is proportional to the intensity of the incident pulse. This can be described in the frequency-domain by $P(\omega_{\mathrm{THz}}) = \varepsilon_{\mathrm{o}}\chi^{(2)}E(\omega_{\mathrm{vis1}})E(\omega_{\mathrm{vis2}})$, where $\omega_{\mathrm{THz}} = |\omega_{\mathrm{vis1}} - \omega_{\mathrm{vis2}}|$. A broad bandwidth (>10 THz) can result owing to the short duration of the incident pulse in the time domain. To date, this mechanism has been used to generate THz radiation in a number of inorganic semiconducting materials including GaAs, GaSe and ZnTe [10–13], as well as in the organic ionic salt 4-*N*, *N*-4-dimethylamino-4′-*N*′-methylstilbazolium tosylate (DAST) [14]. In addition to the size of the second-order susceptibility which determines the magnitude of the induced polarization and therefore directly determines the efficiency of the process [10], the conversion efficiency is governed by the phase matching condition between the induced THz field and the optical fields (equivalent to $k_{\mathrm{vis2}} = k_{\mathrm{vis1}} \pm k_{\mathrm{THz}}$). For this condition to be satisfied, the phase velocity of the THz pulse must be matched to the group velocity of the visible/near-infrared pulse, and therefore requires the matching of the refractive indices for the different fields. The difficulty in achieving phase matching over a broad band of THz frequencies provides a fundamental limitation.

3.2. Ultra-fast charge transport

THz radiation can also be generated by the acceleration of photoexcited electron-hole pairs in semiconductor structures. Here an ultrafast visible/near-infrared pulse of photon energy greater than the semiconductor bandgap, creates electron–hole pairs close to the surface of the generation crystal. These can be accelerated by an appropriate electric field and the resulting changing dipole leads to generation of a THz pulse.

Typically, suitable surface fields are realized in two ways. Figure 4(a) shows a lateral antenna comprising two electrodes deposited onto a semiconductor surface. A large electric field is applied between the electrodes which accelerates the photocarriers generated by the incident laser pulse focused between the electrodes. This technique was introduced by Auston [15] and has been considerably developed subsequently [16]. A related device uses MBE to produce wide bandwidth *p*–i–*n vertical* diode emitters. MBE allows the fabrication of layered semiconductor structures providing considerable flexibility in the design of the bandstructure profile, together with control of doping profiles and carrier densities in the vertical direction (something which is difficult to achieve laterally). Appropriate bandstructure engineering allows modification of the emission bandwidth [17].

A second mechanism is illustrated in figure 4(b), first demonstrated by Zhang *et al* [18, 19]. In this situation, ultrafast charge transport is driven by both the intrinsic electric

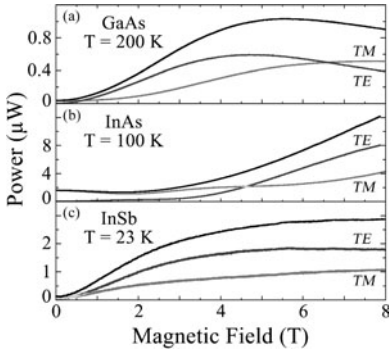

Figure 5. Emitted THz power as a function of applied magnetic field for bulk GaAs, InAs, and InSb. The *TE* and *TM* components of the radiation (labelled) are shown together with the total radiated power. The measurement temperature is chosen in each case to maximize the THz power. Wafer details are given in [32].

field perpendicular to the semiconductor surface [20, 21] and by differences in the electron and hole mobilities (photo-Dember effect) [22–25]. The emitted power and bandwidth for this generation mechanism depend critically upon the temperature and properties of the semiconductor crystal, as well as the energy, pulse width and flux of the incident laser pulse. Recently, there has been enormous interest in this mechanism, which forms the basis for our discussion in section 4, following the demonstration that an external magnetic field can be used to enhance the emitted THz power by over an order of magnitude [26–32]. The mechanism for this enhancement has only recently been explained fully and is now forming the basis for the design of new types of THz emitters.

4. Surface field generation

4.1. Introduction

In this section we focus on THz radiation generated via ultrafast charge transport perpendicular to a semiconductor surface. (The polarization effects leading to optical rectification are negligible for the crystal orientations and photon energies used in the experimental results discussed here.) In addition to the interest in exploiting such transients for the emerging applications of coherent THz spectroscopy [33, 34] and imaging [35], observation of the resulting electric-field transients provides a powerful, non-contact method to study hot carrier dynamics [36], collective processes [37] and material properties of semiconductors, with sub-picosecond time resolution.

4.2. Experimental details

Figure 5 shows the typical THz emission as a function of magnetic field for GaAs, InAs and InSb [29, 30, 32]. The three semiconductor surfaces were excited at an angle of 45° to the surface normal by 2 nJ pulses of 1.6 eV photons from a mode-locked Ti-sapphire laser. The emitted THz radiation was collected parallel to the applied magnetic field and perpendicular to the incident beam as shown in figure 6. Emission was measured both by an incoherent bolometeric detection scheme and also by coherent electro-optic sampling. As expected from the geometry of the experiment, the emitted THz radiation is completely *TM*-polarized in the absence of a magnetic field because the photocarriers accelerate perpendicular to the semiconductor surface. However, as the magnetic field is increased, a *TE* component

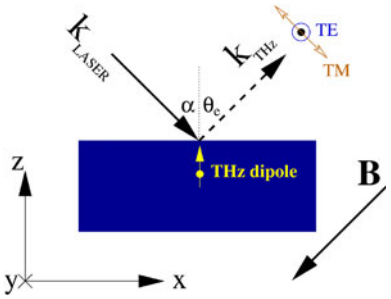

Figure 6. Schematic diagram of the experimental geometry. An fs laser pulse is incident on the semiconductor surface at angle α, leading to a THz dipole. The emitted THz radiation is measured at angle θ_e. The direction of the applied magnetic field is shown by the vector $\boldsymbol{B}$. Figure 5 data has $\alpha = \theta_e = 45^\circ$.

is introduced and the emitted THz radiation becomes elliptically polarized. Both *TE* and *TM* power show significant enhancement in a magnetic field (figure 5), with electro-optic sampling used to demonstrate that the radiation is coherent.

The dependence of the *TM* and *TE*-polarized THz fields on the applied magnetic field, and the maximum emitted THz power, differs significantly between semiconductor surfaces. A nearly monotonic increase in both THz fields is seen in InAs, whilst peaks in the emission are observed in GaAs and InSb. This behaviour, however, does not simply reflect the different carrier concentrations or effective masses in these materials [32].

4.3. Discussion

To understand the carrier dynamics following absorption of a visible/near-infrared pulse, and explain the enhancement of THz emission in magnetic field, Johnston *et al* [38, 39] developed a three-dimensional semi-classical Monte Carlo simulation. A full three-dimensional analysis is required since the magnetic field will alter the charge density distribution in the plane perpendicular to the velocity of the carriers. In this model, the time derivative of the total current is used as a source term in Maxwell's equations, which allows calculation of the electric-field wave forms (and hence spectra) of the THz frequency transient produced from the semiconductor surfaces. Figure 7 shows the time derivatives of the ensemble average current perpendicular to the sample surface, $\partial \boldsymbol{j}_z/\partial t$, for GaAs and InAs. The THz internal field is proportional to $\partial \boldsymbol{j}_z/\partial t$, and has a peak value in *n*-type InAs which is four times that in *n*-type GaAs. This 16-fold power difference agrees well with experiments on such samples (e.g., 20-fold in [28]).

If the semiconductor surface energy bands lie within the bulk bandgap, Fermi level pinning and band-bending occur [40], leading to the formation of a surface depletion or accumulation region. The resulting electric field will separate photo-excited electrons and holes, forming a dipole perpendicular to the surface that can emit THz radiation. By changing from *n*-type to *p*-type doping, the field direction is reversed producing a change in dipole polarity and hence a change in sign of the THz transient.

A photo-Dember field can also occur at a semiconductor surface after photoexcitation [22]. Two factors lead to this field: a difference in diffusion coefficients for electrons and holes, and a structural asymmetry. In a typical semiconductor, electrons have a larger diffusion coefficient than holes. After photo-excitation, the electron population diffuses more rapidly than the hole population but in the absence of a surface boundary, there is no net dipole field, since the centre of charge does not change. In the vicinity of the surface, however, reflection or capture causes the net electron and hole charge centres to move away from the surface.

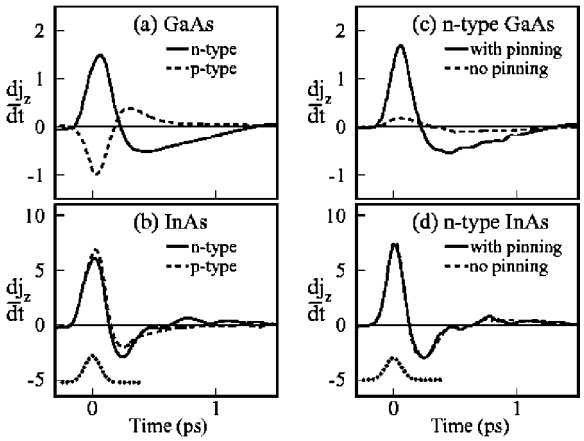

Figure 7. Time derivatives of the z-components of the simulated average current. Graphs (a) and (b) compare n-type (solid lines) and p-type (dashed lines) GaAs and InAs, respectively. Graphs (c) and (d) compare simulations with (solid lines), and without (dashed lines), Fermi level pinning in (c) n-type GaAs and (d) n-type InAs. The dotted curve represents the intensity profile of the exciting laser pulse.

The greater diffusivity of the electrons produces a perpendicular dipole which leads to THz emission. In this case, changing the semiconductor doping from n- to p-type has no effect on the sign of the emitted THz pulse.

Results for simulations of p-type GaAs and InAs are also included in figures 7(a) and (b). For p-type GaAs (figure 7(a)), the polarity of the THz transient changes sign and the wave form is reduced in amplitude, in good agreement with experiments [23, 24, 41], which suggests a surface field mechanism. For InAs (figure 7(b)) there is only a small change between n-type and p-type samples, again consistent with the experimental results [24], which suggests a photo-Dember emission mechanism.

Figures 7(c) and (d) present a more quantitative analysis of the contributions of the surface field and photo-Dember generation mechanisms to emission from n-type GaAs and InAs. In each plot, the dashed line represents a sample in which the Fermi level is not pinned and so there is no surface depletion field. It therefore represents the pure photo-Dember field emission mechanism. By integrating the power spectra of the GaAs waveforms we find that less than 10% of radiated power is generated by the photo-Dember mechanism. In contrast, the n-type InAs wave forms presented in figure 7(d) are indistinguishable, indicating close to 100% photo-Dember emission.

These simulations reproduce the larger THz electric-field amplitudes (and hence powers) observed experimentally in InAs when compared with GaAs, and demonstrate that InAs is primarily a photo-Dember emitter while GaAs is primarily a surface field emitter.

4.4. Magnetic field enhancement

In order to explain the dramatic enhancement of THz emission with magnetic field (figure 5), Johnston *et al* [38, 39] modelled the carrier dynamics for both InAs and GaAs in magnetic fields ranging from 0 to 8 T, and calculated the amplitude and three-dimensional orientation of the THz emitting dipole. The coupling of the radiation out of the semiconductor is strongly affected by the dipole orientation with respect to the semiconductor surface [38, 39, 42].

Figures 8(a) and (b) show the simulated time derivatives of the current densities in n-type GaAs and n-type InAs, respectively, during and after photoexcitation. The dashed lines show

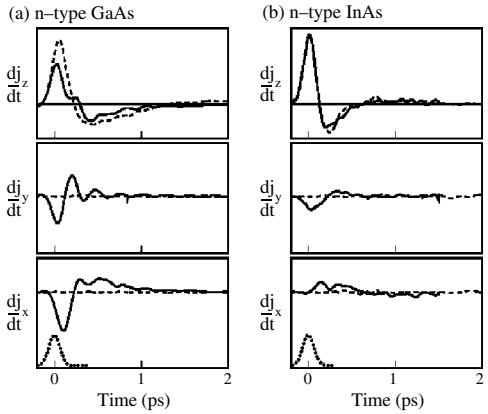

Figure 8. Three spatial components of the time derivative of average current density for *n*-type (a) GaAs and (b) InAs at $B = 0$ T (dashed lines) and $B = 8$ T (solid lines). The dotted curve represents the intensity profile of the exciting laser pulse. The vertical axis range in (b) is 4× that of (a).

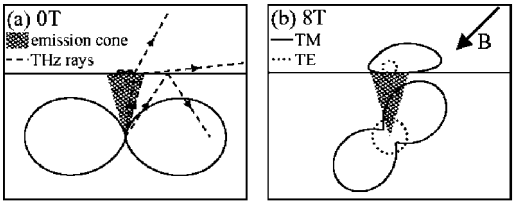

Figure 9. Calculated polar radiation patterns for GaAs at (a) $B = 0$ T and (b) $B = 8$ T. The horizontal lines represent the semiconductor surface. The 'bow tie' pattern below the surface shows the radiation within the semiconductor; the pattern above the surface shows the free-space emission. The vector $\boldsymbol{B}$ indicates the magnetic field direction.

the situation with no magnetic field present. In this case, the only net acceleration of carriers ($\partial \boldsymbol{j}/\partial t$) occurs in the z-direction since the only asymmetries in the system are the surface boundary and surface electric field, both of which are rotationally symmetric about the z-axis. The solid lines represent a simulation with a magnetic field of 8 T. Although there is little change to the strength of the dipole as the magnetic field is increased, the x and y components of $\partial \boldsymbol{j}/\partial t$ show that the Lorentz force produces a net acceleration of carriers in the x–y plane and rotates the THz dipole. This is much less pronounced in InAs compared with GaAs, however. This is because the 1.55-eV incident photons excite the electrons high into the InAs conduction band, with the result that inter-valley scattering is a much more important electron scattering process in InAs than in GaAs. The large effective mass of electrons scattered into the L valleys limits the rotation of the photogenerated dipole, and hence the relative magnitude of the lateral $\partial \boldsymbol{j}/\partial t$ components.

In order to be measured in free space, the THz radiation generated within the semiconductor of refractive index $n_\mathrm{i} \sim 3.5$ must be transmitted into a medium of refractive index $n_\mathrm{e} \sim 1.0$. It is clear that any radiation generated outside a cone of about $\theta_\mathrm{i} \sim 17^\circ$ (measured from the surface normal) will be totally internally reflected. To calculate the emission pattern resulting from radiation generated within this cone, the Fresnel transmission coefficients must be considered [39].

Figure 9(a) shows the 'bow-tie' radiation pattern of the power produced inside the GaAs at $B = 0$ T, together with the radiation pattern emitted from GaAs into free space. The amount of radiation emitted is very low because of the small overlap between the (shaded) emission

cone and the internal radiation pattern. The excited spot can be considered as a distribution of point dipoles, with relative phases set by the phase variation across the laser pulse, causing collimation in the reflection direction [43]. Figure 9(b) shows the situation at $B = 8$ T. The internal radiation pattern shows the rotation of the *TM*-emitting THz dipole from being parallel to the z-axis to being approximately perpendicular to the magnetic-field vector. A *TE* component also emerges. In this case there is now considerable overlap between the internal radiation pattern and the emission cone, and hence the corresponding free-space radiation pattern is much larger. For InAs, there is only a small rotation of the THz dipole (not shown) and hence the enhancement of the free-space radiation is much less. The enhancement in total THz power emitted at $\theta_e = 45^\circ$ between 0 and 8 T has been measured experimentally to be $35\times$ for GaAs [32, 38] and $8\times$ for InAs [29]. Here, the calculated values are $15\times$ and $4\times$, respectively. These results are in reasonable agreement considering the simplicity of the semi-classical simulation, and possible differences between the experimental and simulation parameters.

4.5. Conclusions

We have discussed a semiclassical Monte Carlo model which simulates the dynamics of extrinsic and photoexcited electrons and holes on a sub-picosecond timescale. The simulation shows that after excitation with a laser pulse, the primary THz emission mechanism from InAs is based on the photo-Dember effect, while surface depletion fields dominate in GaAs. The effect of magnetic field on these systems has been calculated and the experimentally observed enhancement of THz power with magnetic field is found to be predominantly caused by a reorientation of the THz dipole with respect to the surface dielectric boundary, rather than by an increase in the dipole strength. Once transmission through the semiconductor–air dielectric interface is considered, the experimentally observed enhancement in emission is reproduced.

These results suggest that a magnetic field is not necessary to obtain an order-of-magnitude enhancement in THz power. A similar enhancement should be produced by reducing the effective refractive index of the semiconductor or by modifying the dipole orientation with respect to the dielectric–air interface by way of a prism or lens [43]. By reorienting the THz dipole towards the semiconductor surface, the emitter then resembles the lateral antennae discussed in section 3.2.

5. Overview of applications

The development of coherent THz time-domain spectroscopy discussed in section 2, together with recent proving experiments, have demonstrated the potential for THz imaging and spectroscopy across the physical, biological and medical sciences (figure 10) [35]. Biomedical THz imaging, in particular, has attracted much attention [44]. Different biological tissues have different absorption spectra and refractive indices in the THz range. These criteria serve as new contrast mechanisms from which images of live tissue, and abnormalities in such tissue, may be obtained. The non-ionizing nature of THz and its ability to distinguish different soft tissue types may lead to significant advantages over other imaging modalities in specific medical applications. This research is on-going following the first demonstration of THz imaging of biological tissue (a leaf) [7], and subsequent imaging of, for example, an extracted human tooth [45] and sub-epidermal basal cell carcinoma [46].

This field is wide-ranging and cross-disciplinary, however, and in addition to the biomedical applications there is relevance to molecular and nanostructure spectroscopy, high bandwidth electronic communications, local oscillators for astronomy, and diagnostic testing, *inter alia*.

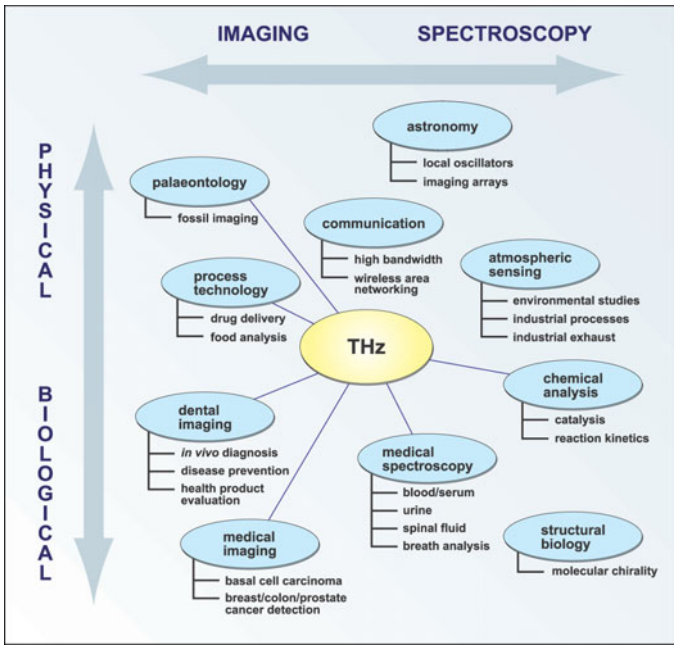

Figure 10. Schematic overview showing some of the proved and potential applications of THz imaging and spectroscopy across the physical, biological and medical sciences.

The potential for commercial exploitation of this technology may be currently restricted by the high cost of the femtosecond pulsed lasers, and the convenience and practicality of using such bulky assemblies. For these reasons, there is a strong driving force for the fabrication of cheap, solid-state THz emitters and detectors, and the recent reports of quantum cascade lasers operating at 4.4 THz (albeit at cryogenic temperatures) [5, 6] are very encouraging for the continuing development of THz photonics over the next decade.

Acknowledgments

We are grateful for numerous discussions with A Corchia, A R Dowd, R McLaughlin, Y-C Shen, D M Whittaker, D D Arnone and M Pepper. AGD and EHL acknowledge the support of the Royal Society and Toshiba Research Europe Limited, respectively. This work was supported by the Engineering and Physical Sciences Research Council, and the Rutherford Appleton Laboratory.

References

[1] See, for example, Chamberlain J M, Miles R E, Collins C E and Steenson D P 1997 *New Directions in Terahertz Technology* ed J M Chamberlain and R E Miles (NATO ASI Series, Kluwer) and references therein
[2] Crowe T W, Grein T C, Zimmerman R and Zimmerman P 1996 *IEEE Microw Guided Wave Lett*. **6** 207–8
Eisele H, Rydberg A and Haddad G I 2000 *IEEE Trans. Microw Theory Tech*. **48** 626–31
[3] Faist J, Capasso F, Sivco D L, Sirtori C, Hutchinson A L and Cho A Y 1994 *Science* **264** 553–6
[4] Colombelli R, Capasso F, Gmachl C, Hutchinson A L, Sivco D L, Tredicucci A, Wanke M C, Sergent A M and Cho A Y 2001 *Appl. Phys. Lett*. **78** 2620–2
[5] Köhler R, Tredicucci A, Beltram F, Beere H E, Linfield E H, Davies A G, Ritchie D A, Iotti R C and Rossi F 2002 *Nature* **417** 156–9
[6] Rochat M, Ajili L, Willenberg H, Faist J, Beere H E, Davies A G, Linfield E H and Ritchie D A 2002 *Appl. Phys. Lett*. **81** 1381–3

[7] Hu B B and Nuss M C 1995 *Opt. Lett.* **20** 1716–8
[8] See Nuss M C and Orenstein J 1998 *Millimeter and Submillimeter Wave Spectroscopy of Solids* ed G Grüner (Berlin: Springer) and references therein
[9] Wu Q, Litz M and Zhang X-C 1996 *Appl. Phys. Lett.* **68** 2924–6
[10] Ma X F and Zhang X-C 1993 *J. Opt. Soc. Am.* B **10** 1175–9
[11] Seeta P N, Greene B I and Chuang S L 1993 *Appl. Phys. Lett.* **63** 3482–4
[12] Rice A, Jin Y, Ma X F and Zhang X-C 1994 *Appl. Phys. Lett.* **64** 1324–6
[13] Corchia A, Ciesla C M, Arnone D D, Linfield E H, Simmons M Y and Pepper M 2000 *J. Mod. Optics.* **47** 1837–45
[14] Han P Y, Tani M, Pan F and Zhang X-C 2000 *Opt. Lett.* **25** 675–7
Walther M, Jensby K, Heiding S R, Takahashi H and Ito H 2000 *Opt. Lett.* **25** 911–3
[15] Auston D H 1975 *Appl. Phys. Lett.* **26** 101–3
[16] Grischkowsky D R 2000 *IEEE J. Sel. Topics Quantum Electron.* **6** 1122–35
Zhao G, Schouten R N, van der Valk N, Th Wenckebach W and Planken P C M 2002 *Rev. Sci. Instrum.* **73** 1715
[17] Leitenstorfer A, Hunsche S, Shah J, Nuss M C and Knox W H 1999 *Phys. Rev. Lett.* **82** 5140–3
[18] Zhang X-C, Hu B B, Darrow J T and Auston D H 1990 *Appl. Phys. Lett.* **56** 1011
[19] Hu B B, Zhang X-C and Auston D H 1991 *Phys. Rev. Lett.* **67** 2709
[20] Zhang X-C and Auston D H 1992 *J. Appl. Phys.* **71** 326
[21] Dekorsy T, Pfeifer T, Kütt W and Kurz H 1993 *Phys. Rev.* B **47** 3842
[22] Dember H 1931 *Phys. Z.* **32** 554
Dember H 1931 *Phys. Z.* **32** 856
Dember H 1932 *Phys. Z.* **33** 207
[23] Dekorsy T, Auer H, Bakker H J, Roskos H G and Kurz H 1996 *Phys. Rev.* B **53** 4005
[24] Gu P, Tani M, Kono S and Sakai K 2000 *8th Int. Conf. on Terahertz Electronics (VDE Verlag, Berlin-Offenbach)* pp 63–65
[25] Kono S, Gu P, Tani M and Sakai K 2000 *Appl. Phys.* B **71** 901
[26] Sarukura N, Ohtake H, Izumida S and Liu Z 1998 *J. Appl. Phys.* **84** 654
[27] Izumida S, Ono S, Liu Z, Ohtake H and Sarukura N 1999 *Appl. Phys. Lett.* **75** 451
[28] Weiss C, Wallenstein R and Beigang R 2000 *Appl. Phys. Lett.* **77** 4160
[29] McLaughlin R, Corchia A, Johnston M B, Chen Q, Ciesla C M, Arnone D D, Jones G A C, Linfield E H, Davies A G and Pepper M 2000 *Appl. Phys. Lett.* **76** 2038
[30] Corchia A, McLaughlin R, Johnston M B, Whittaker D M, Arnone D D, Linfield E H, Davies A G and Pepper M 2001 *Phys. Rev.* B **64** 205204
[31] Heyman J N, Neocleous P, Hebert D, Crowell P A, Müller T and Unterrainer K 2001 *Phys. Rev.* B **64** 085202
[32] Johnston M B, Corchia A, Dowd A, Linfield E H, Davies A G, McLaughlin R, Arnone D D and Pepper M 2001 *Physica* E **13** 896–9
[33] Auston D H and Cheung K P 1984 *J. Opt. Soc. Am.* B **2** 606
[34] Han P Y, Cho G C and Zhang X-C 2000 *Opt. Lett.* **25** 242
[35] See, for example Mittleman D M, Gupta M, Neelamani R, Baraniuk R G, Rudd J V and Koch M 1999 *Appl. Phys.* B **68** 1085–94
Jiang Z and Zhang X-C 1999 *IEEE Trans. Microw Theory Tech.* **47** 2644–50
[36] Leitenstorfer A, Hunsche S, Shah J, Nuss M C and Knox W H 2000 *Phys. Rev.* B **6116** 642
[37] Kersting R, Heyman J N, Strasser G and Unterrainer K 1998 *Phys. Rev.* B **58** 4553
[38] Johnston M B, Whittaker D M, Corchia A, Davies A G and Linfield E H 2002 *J. Appl. Phys.* **91** 2104–6
[39] Johnston M B, Whittaker D M, Corchia A, Davies A G and Linfield E H 2002 *Phys. Rev.* B **65** 165301
[40] Yu P Y and Cardona M 1996 *Fundamentals of Semiconductors, Physics and Material Properties* (Berlin: Springer) ch 8, pp 448–53
[41] Spicer W E, Liliental-Weber Z, Weber E, Newman N, Kendelewicz T, Cao R, McCants C, Mahowald P, Miyano K and Lindau I 1988 *J. Vac. Sci. Technol.* B **6** 1245
[42] Shan J, Weiss C, Wallenstein R, Beigang R and Heinz T F 2001 *Opt. Lett.* **26** 849
[43] Johnston M B, Whittaker D M, Dowd A, Davies A G, Linfield E H, Li X and Ritchie D A 2002 *Opt. Lett.* at press
[44] See, for example, *Proceedings of the First International Conference on Biomedical Imaging and Sensing Applications of THz Technology (Leeds, UK, 2001)* (this issue) and references therein
[45] Ciesla C M, Arnone D D, Corchia A, Crawley D, Longbottom C, Linfield E H and Pepper M 2000 *Commercial and Biomedical Applications of Ultrafast Lasers II*, *Proc. SPIE* vol 3934, ed J Neev and M K Reed (Bellingham, WA: SPIE) pp 73–81
[46] Woodward R M, Cole B, Wallace V P, Arnone D D, Pye R, Linfield E H, Davies A G and Pepper M 2001 *Technical Digest of the Conference on Lasers and Electro-Optics (Optical Society of America, Baltimore)*